Acta Crystallographica Section D
Biological Crystallography
ISSN 0907-4449

Structure of peptidyl-tRNA hydrolase 2 from *Pyrococcus horikoshii* OT3: insight into the functional role of its dimeric state

Katsumi Shimizu,[a] Chizu Kuroishi,[b] Mitsuaki Sugahara[c] and Naoki Kunishima[a]*

[a]Advanced Protein Crystallography Research Group, RIKEN SPring-8 Center, Harima Institute, 1-1-1 Kouto, Sayo-cho, Sayo-gun, Hyogo 679-5148, Japan, [b]Structurome Research Group, RIKEN SPring-8 Center, Harima Institute, 1-1-1 Kouto, Sayo-cho, Sayo-gun, Hyogo 679-5148, Japan, and [c]Structural Biophysics Laboratory, RIKEN SPring-8 Center, Harima Institute, 1-1-1 Kouto, Sayo-cho, Sayo-gun, Hyogo 679-5148, Japan

Correspondence e-mail: kunisima@spring8.or.jp

Received 5 November 2007
Accepted 25 January 2008

PDB References: peptidyl-tRNA hydrolase 2, form 1, 1wn2, r1wn2sf; form 2, 2d3k, r2d3ksf.

Peptidyl-tRNA hydrolases catalyze the hydrolytic removal of the peptidyl moiety from the peptidyl-tRNA molecule to prevent misreading during translation. Here, the expression, purification, crystallization and X-ray diffraction study of peptidyl-tRNA hydrolase 2 from *Pyrococcus horikoshii* OT3 (*Ph*Pth2) are described. The crystal structures were determined as similar biological dimers in two different forms: $P4_12_12$ at 1.2 Å resolution (form 1) and $P4_322$ at 1.9 Å resolution (form 2). In the form 1 structure, the asymmetric unit contains one *Ph*Pth2 subunit and a crystallographic twofold axis defines the dimeric association with the cognate subunit. In the form 2 structure, there are two *Ph*Pth2 subunits in the asymmetric unit that make a similar dimer with a noncrystallographic twofold axis. In order to evaluate the thermodynamic stability, the intra-protomer and inter-protomer interactions of *Ph*Pth2 were analyzed and compared with those of other Pth2-family members. The thermodynamic parameters show that the large number of ion pairs compared with family members from other mesophilic organisms would contribute to the thermostability of *Ph*Pth2. The structural difference between the two dimers was quantitatively evaluated by a multiple C^{α}-atom superposition. A significant structural difference between the two dimers was observed around the putative active site of this enzyme. A rigid-body rotation takes place so as to retain the dimeric twofold symmetry, suggesting positive cooperativity upon tRNA binding. The mechanism of ligand binding was further investigated using a docking model with a tRNA molecule. The docking study suggests that the binding of tRNA requires its simultaneous interaction with both subunits of the *Ph*Pth2 dimer.

1. Introduction

During the process of protein translation, a premature peptidyl-tRNA may dissociate from the ribosome before the completion of mRNA readout by reaching the stop codon (Meinnel *et al.*, 1993; Schmitt *et al.*, 1997). The accumulation of such peptidyl-tRNA in cells leads to reduced efficiency of translation and eventually impairs translation initiation by depletion of tRNA (Menninger, 1976). Peptidyl-tRNA hydrolase (Pth) catalyzes the hydrolytic removal of the peptidyl moiety from the peptidyl-tRNA molecule, allowing the reuse of the resultant free tRNA in protein biosynthesis.

The enzyme Pth can be classified into two types: peptidyl-tRNA hydrolase 1 (Pth1) and peptidyl-tRNA hydrolase 2 (Pth2). These two enzymes are ubiquitous in nature; Pth1 enzymes have been identified in bacteria and eukaryotes (Kössel, 1970; Brun *et al.*, 1971; Menez *et al.*, 2002), while Pth2

enzymes are present in eukaryotes and archaea (Rosas-Sandoval *et al.*, 2002; Fromant *et al.*, 2003). The number of amino-acid residues constituting the polypeptide chain is about 190 in Pth1 and about 120 in Pth2. These two enzymes do not show any significant sequence identity. The first crystal structure of Pth1 to be determined was that of the *Escherichia coli* enzyme, which revealed a single α/β globular domain built around a twisted mixed β-sheet (Schmitt *et al.*, 1997). More recently, the first crystal structure of human Pth2 was determined (hPth2; de Pereda *et al.*, 2004). The crystal structure of hPth2 shows a characteristic homodimer of a monomeric protomer comprising a mixed β-sheet sandwiched by two groups of two α-helices and lacks any three-dimensional structural similarity to the structure of Pth1. Other structural studies carried out to date include the crystal structure of the *Sulfolobus solfataricus* enzyme (*Ss*Pth2) and the solution structure of the *Archaeglobus fulgidis* enzyme (*Af*Pth2). A site-directed mutagenesis study showed that the three conserved residues Lys18, Asp86 and Thr90 in *Ss*Pth2 may be involved in catalysis (Fromant *et al.*, 2005). A structural comparison between *Af*Pth2 and other Pth2-family members allowed us to predict the catalytic residues and the tRNA-interaction region (Powers *et al.*, 2005). However, the structure–thermostability and structure–function relationships in Pth2 largely remain unexplored.

In this paper, we present the crystal structure of Pth2 from *Pyrococcus horikoshii* OT3 (*Ph*Pth2). The hyperthermophilic archeon *P. horikoshii* has one of the highest optimum growth temperatures (T_{ogt}) at 368 K. Structures of two crystal forms have been determined: form 1, which belonged to space group $P4_12_12$ and diffracted to 1.2 Å resolution, and form 2, which belonged to space group $P4_322$ and diffracted to 1.9 Å resolution. Both forms contain similar biological dimers and forms 1 and 2 contain one and two subunits in the asymmetric unit, respectively. The thermodynamic stability of Pth2-family members is discussed based on thermodynamic parameters (Gibbs free energy, entropy and number of ion pairs) using the available crystal structures, which may provide insight into the structure–thermostability relationship of this enzyme. A structural comparison between the two *Ph*Pth2 dimers was carried out with the goal of understanding the ligand recognition of this enzyme. The ligand-binding mode has been visualized using a docking model of *Ph*Pth2 with *Saccharomyces* tRNA (PDB code 1evv) to investigate the structure–function relationship.

2. Experimental

2.1. Protein expression and purification

Peptidyl-tRNA hydrolase 2 from *P. horikoshii* OT3 (*Ph*Pth2; PH1539) has a molecular weight of 13.4 kDa and consists of 121 amino-acid residues. *E. coli* BL21-CodonPlus (DE3)-RIL cells were transformed with the recombinant plasmid pET-11a carrying a gene encoding *Ph*Pth2 (residues 1–121) and grown at 310 K in Luria–Bertani medium containing 50 µg ml^{-1} ampicillin for 20 h. The cells were harvested by centrifugation at 20 000*g* for 4 min and suspended in 20 m*M* Tris–HCl pH 8.0 (buffer *A*) containing 500 m*M* NaCl, 5 m*M* 2-mercaptoethanol and 1 m*M* phenylmethylsulfonyl fluoride. The cells obtained were disrupted by sonication and heated at 363 K for 11.5 min. After the heat treatment, cell debris and denatured protein were removed by centrifugation at 277 K (21 600*g*, 30 min) and the supernatant was used as the crude extract for purification. The crude extract was desalted using a HiPrep 26/10 desalting column (Amersham Biosciences) and applied onto a Super Q Toyopearl 650M column (Tosoh) equilibrated with buffer *A*. Proteins were eluted with a linear gradient of 0–0.3 *M* NaCl. After replacement with buffer *A*, the fraction containing *Ph*Pth2 was subjected to a Resource Q column (Amersham Biosciences) equilibrated with buffer *A* and eluted with a linear gradient of 0–0.3 *M* NaCl in buffer *A*. After buffer replacement with 10 m*M* phosphate–NaOH pH 7.0 (buffer *B*), the fraction containing *Ph*Pth2 protein was applied onto a Bio-Scale CHT-20-I column (Bio-Rad) equilibrated with buffer *B* and eluted with a linear gradient of 10–300 m*M* buffer *B*. The fraction containing *Ph*Pth2 was concentrated by ultrafiltration (Vivaspin, 5 kDa cutoff, Vivascience) and loaded onto a HiLoad 16/60 Superdex 75 prep-grade column (Amersham Biosciences) equilibrated with buffer *A* containing 0.2 *M* NaCl. The homogeneity and identity of the purified sample were assessed by SDS–PAGE and N-terminal sequence analysis. Finally, the purified *Ph*Pth2 protein was concentrated to 63.9 mg ml^{-1} by ultrafiltration and kept at 203 K.

2.2. Dynamic light scattering

A dynamic light-scattering (DLS) experiment was carried out using a DynaPro MS/X instrument (Protein Solutions) to examine the oligomeric state of the purified *Ph*Pth2. The protein concentration of the solution was 1.0 mg ml^{-1} in 20 m*M* Tris–HCl buffer pH 8.0 containing 200 m*M* NaCl. Several measurements were taken at 291 K and analyzed using *DYNAMICS* software v.3.30 (Protein Solutions). A particle-size distribution with polydispersity of 20.6% was observed and the molecular weight was estimated to be 25.3 kDa, which is consistent with a dimeric state of *Ph*Pth2 in solution.

2.3. Crystallization and preliminary X-ray diffraction study

In order to obtain protein crystals that were suitable for X-ray diffraction experiments, initial screening of crystallization conditions was carried out using the TERA automatic crystallization system (Sugahara & Miyano, 2002), which is based on the oil-microbatch method (Chayen *et al.*, 1990), using NUNC HLA plates (Nalge Nunc International). After the initial screening, we optimized the crystallization conditions and obtained two different conditions: (i) 16.5%(*w*/*v*) PEG 20K as precipitant, 0.1 *M* CHES–HCl pH 9.24 as buffer and (ii) 10%(*w*/*v*) PEG 8K as precipitant, 0.1 *M* MES–NaOH pH 6.0 as buffer and 0.2 *M* zinc acetate as an additive. A 0.5 µl aliquot of the optimized precipitant solution was mixed with 0.5 µl protein solution (63.9 mg ml^{-1} protein, 0.2 *M* NaCl,

Table 1
Summary of data-collection and refinement statistics.

Values in parentheses are for the highest shell.

	Form 1	Form 2
Data collection		
X-ray source	BL26B1, SPring-8	BL26B2, SPring-8
Wavelength (Å)	1.0	1.0
Temperature (K)	100	100
Space group	$P4_12_12$	$P4_322$
Unit-cell parameters (Å)		
a	49.7	59.9
c	85.8	128.2
Content of ASU	Protomer	Dimer
Resolution range (Å)	40.0–1.2 (1.24–1.2)	40.0–1.9 (1.97–1.9)
No. of reflections measured	308946	164229
No. of unique reflections	34396	19193
R_{merge} (%)	5.5 (33.6)	7.8 (43.6)
Completeness (%)	100 (100)	99.9 (100)
$R_{sym}(I)$ (%)	5.3 (31.9)	7.3 (41.1)
$I/\sigma(I)$	15.4 (4.7)	10.8 (4.4)
Refinement statistics		
Resolution range (Å)	35.1–1.2 (1.28–1.2)	32.6–1.9 (2.2–1.9)
No. of reflections	34325	19146
R (%)	19.3 (22.2)	20.8 (23.0)
R_{free}† (%)	21.5 (24.2)	25.5 (25.7)
R.m.s. deviations from ideal geometry		
Bond distances (Å)	0.006	0.005
Bond angles (°)	1.5	1.2
Ramachandran plot, residues in (%)		
Most favoured region	94.2	91.9
Allowed region	5.8	8.1
Generously allowed region	0	0
Disallowed region	0	0
Estimated coordinate error (Å)	0.13	0.22

† R_{free} is calculated for a subset of reflections (5%) excluded from all stages of refinement.

20 m*M* Tris–HCl pH 8.0) in a well of the HLA plate. Subsequently, the 1 µl crystallization drop was covered with 15 µl of a 7:3(*v*:*v*) mixture of paraffin and silicon oils, allowing slow evaporation of water in the drop, and stored at 291 K. Crystals with suitable dimensions for X-ray diffraction study were reproducibly obtained using the TERA system. The crystals were flash-cooled in a nitrogen-gas stream at 100 K using an oil-based cryoprotectant comprising 90% Paratone-N and 10% glycerol by weight (Kwong & Liu, 1999). Preliminary X-ray diffraction experiments were carried out using a microfocus rotating-anode X-ray generator (Rigaku MicroMax007) equipped with a Rigaku R-AXIS VII image-plate detector. The space group and unit-cell parameters obtained from the optimized crystallization conditions (i) and (ii) are (i) $P4_12_12$ with $a = 49.7$, $c = 85.8$ Å (crystal form 1) and (ii) $P4_322$ with $a = 59.9$, $c = 128.2$ Å (crystal form 2).

2.4. Data collection and structure determination

X-ray diffraction data sets were collected from the form 1 and 2 crystals at SPring-8 beamlines BL26B1 and BL26B2, respectively (Ueno *et al.*, 2006). The detectors used were a Rigaku R-AXIS V image-plate detector and a Rigaku Jupiter 210 CCD detector for forms 1 and 2, respectively. The SPring-8 Precise Automatic Cryo-sample Exchanger (SPACE) automated sample-management system was used for data collection from the form 2 crystal (Ueno *et al.*, 2004). The X-ray diffraction data were integrated and scaled using the programs *DENZO* and *SCALEPACK* (Otwinowski & Minor, 1997). The crystal structures of both forms were solved by the molecular-replacement method using the program *MOLREP* (Vagin & Teplyakov, 1997). To solve the form 1 structure, the coordinates of the crystal structure of *Thermoplasma acidophilum* Pth2 (*Ta*Pth2; PDB code 1rlk) were used as a search model; the form 2 structure was determined using the final coordinates of the form 1 structure (PDB code 1wn2) as a search model. Model building and revision were performed using *QUANTA*2000 (Accelrys Inc.). The program *CNS* v.1.1 (Brünger *et al.*, 1998) was used for structural refinement and electron-density map calculation. The stereochemical quality of the refined final model was evaluated using the program *PROCHECK* (Laskowski *et al.*, 1998). The final structures include 919 protein atoms, one sodium ion and 187 water molecules for the form 1 structure refined at 1.2 Å resolution and 1838 protein atoms, two zinc ions and 244 water molecules for the form 2 structure refined at 1.9 Å resolution. A summary of the data-collection and refinement statistics is given in Table 1.

3. Results and discussion

3.1. Overall structure of *Ph*Pth2

We have established the expression, purification and crystallization of peptidyl-tRNA hydrolase 2 from *P. horikoshii* OT3 (*Ph*Pth2) and determined its crystal structure in two space groups: $P4_12_12$ (crystal form 1) and $P4_322$ (crystal form 2). The asymmetric unit of the form 1 structure contains a

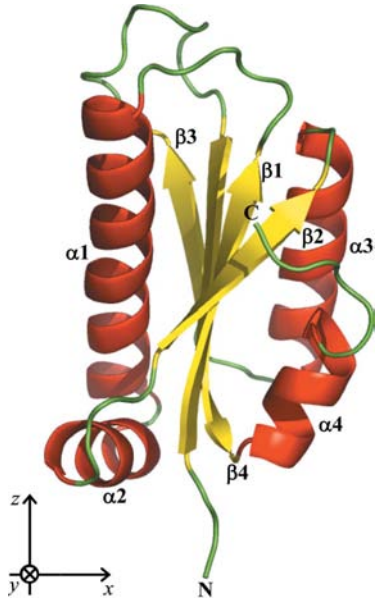

Figure 1
Ribbon diagram of *Ph*Pth2 form 1 protomer. The constituent elements of the secondary structure are shown in red (α-helices), yellow (β-strands) and green (loops). For comparison with other figures, the direction of the projection is shown by the coordinate axes. This figure was generated using *PyMOL* (DeLano, 2002).

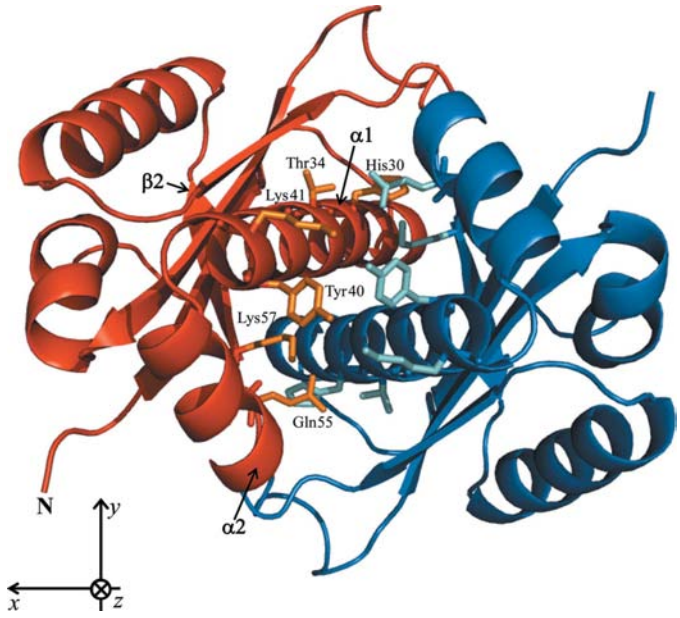

Figure 2
Ribbon diagram of *Ph*Pth2 form 1 dimer viewed along the crystallographic twofold axis. The dimer interface involves the $\alpha1$ and $\alpha2$ helices, the $\alpha2$–$\beta2$ loop and the $\beta2$ strand, which are mainly composed of hydrophobic residues. The residues that make a hydrogen bond between crystal symmetry-related protomers are shown as stick models. For comparison with other figures, the direction of the projection is shown by the coordinate axes. This figure was generated using *PyMOL* (DeLano, 2002).

*Ph*Pth2 protomer (denoted *A*) and two identical protomers are related by a crystallographic twofold axis to form an apparent dimer. The Ramachandran plot shows 94.2% of residues in the most favoured region and 5.8% of residues in additional allowed regions. In the form 2 structure there are two independent *Ph*Pth2 protomers (denoted *A* and *B*) in the asymmetric unit. These two protomers make up a dimer with a noncrystallographic twofold axis similar to that observed in form 1. The Ramachandran plot shows 91.9% of residues in the most favoured region and 8.1% in additional allowed regions. For all polypeptide chains in both forms 1 and 2 electron densities for the N-terminal residues Met1–Lys 3 are missing, probably owing to disorder, and these were not built into the final model, which consisted of residues 4–121.

The *Ph*Pth2 protomer displays the same α/β-fold as previously reported for other Pth2-family members (Fig. 1). Apparent dimeric structures (Fig. 2) are observed in the *Ph*Pth2 crystals. The fact that similar dimers are found in the two different crystal forms suggests a biological relevance of the dimer, which is consistent with the dynamic light-scattering experiment, which showed a dimeric state of *Ph*Pth2 in solution. The dimer interface in form 1 involves the $\alpha1$ and $\alpha2$ helices, the $\alpha2$–$\beta2$ loop and the $\beta2$ strand, which are mainly composed of hydrophobic residues that make a tight hydrophobic core; the residues His30, Thr34, Tyr40, Lys41, Gln55 and Lys57 make hydrogen bonds between the crystal symmetry-related protomers. In form 2, the dimer interface involves the $\beta1$–$\alpha1$ loop, the $\alpha1$ and $\alpha2$ helices, the $\alpha2$–$\beta2$ loop

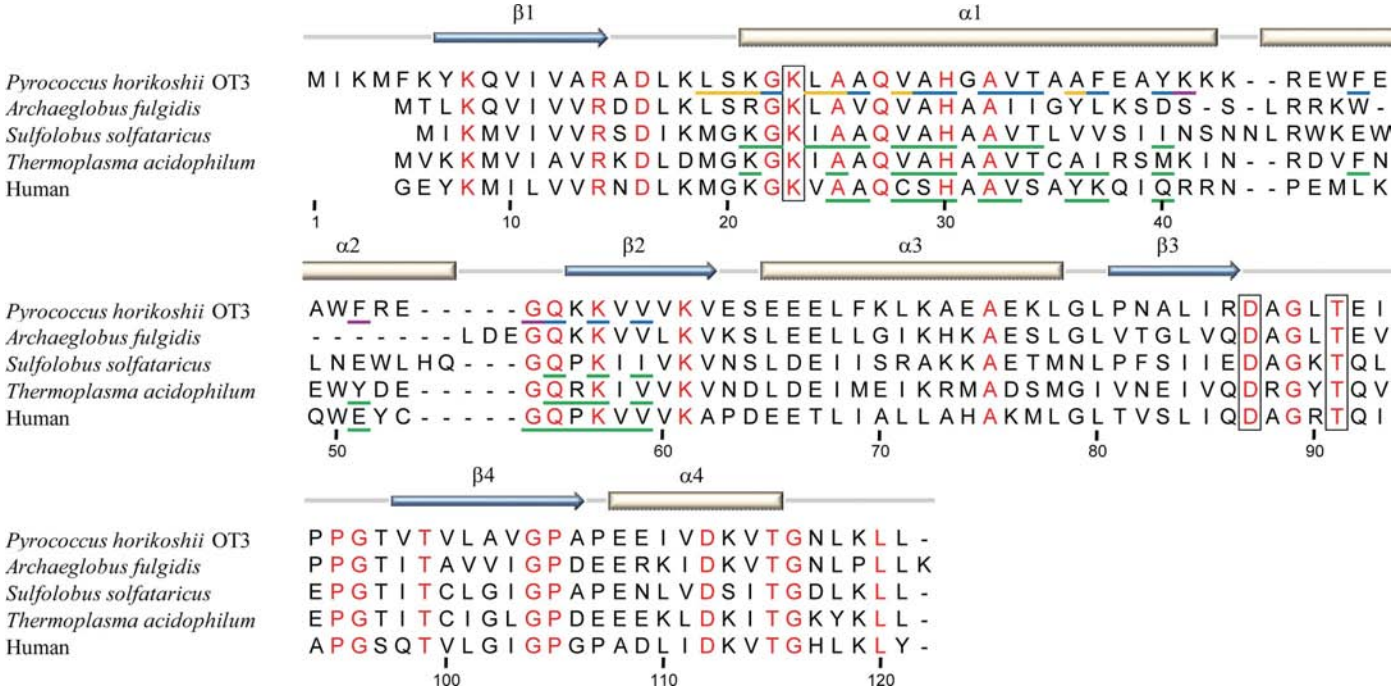

Figure 3
Structure-based amino-acid sequence alignment of *Ph*Pth2 and Pth2-family members. Helices and strands are shown as cylinders and arrows, respectively. The residues coloured red represent residues that are conserved in all organisms. The residues Lys23, Asp87 and Thr91 for *Ph*Pth2 are expected to form a putative active site and the corresponding residues for the five organisms are enclosed in boxes. For *Ph*Pth2, the residues underlined in magenta, orange and blue make dimer interfaces in the form 1, form 2 and both the form 1 and 2 dimers, respectively. For the others, with the exception of *Af*Pth2, the residues underlined in green make dimer interfaces.

and the β2 strand; the residues Leu19, Lys21, His30, Thr34, Gln55 and Lys57 make hydrogen bonds between the local symmetry-related protomers. The dimension of the buried dimer-interface area per protomer is 1026 Å^2 in form 1 and 1101 Å^2 in form 2 and these contact areas occupy 15% and 16% of the total protomer surface area, respectively.

3.2. Structural comparison between *Ph*Pth2 and other Pth2 family members

The sequence similarity between *Ph*Pth2 and other Pth2 members was investigated using a *BLAST* search (Altschul *et al.*, 1990). *Ph*Pth2 (gi:6686200) shares 57% sequence identity (65/114) and an *e* value of 9×10^{-27} with *A. fulgidis* Pth2 (*Af*Pth2; gi:56965973), 50% sequence identity (58/115) and an *e* value of 1×10^{-25} with human Pth2 (hPth2; gi:6807813), 48% sequence identity (57/118) and an *e* value of 3×10^{-27} with *S. solfataricus* Pth2 (*Ss*Pth2; gi:62738521) and 47% sequence identity (54/114) and an *e* value of 5×10^{-26} with *T. acidophilum* Pth2 (*Ta*Pth2; gi:40889674).

The three-dimensional structure of *Ph*Pth2 was compared with other structures of Pth2 family from the PDB using the program *DALI* (Holm & Sander, 1997). The form 1 protomer of *Ph*Pth2 shows high structural similarity to hPth2 protomers (crystal structure; PDB code 1q7s; *Z* score 20.7 and r.m.s.d. 1.3 Å), *Ss*Pth2 (crystal structure; PDB code 1xty; *Z* score 20.7 and r.m.s.d. 1.2 Å) and the *Ta*Pth2 protomer (crystal structure; PDB code 1rlk; *Z* score 20.8 and r.m.s.d. 1.4 Å). The *Af*Pth2 protomer, which has the highest sequence identity to the *Ph*Pth2 form 1 protomer, shows lower scores (NMR structure; PDB code 1rzw; *Z* score 7.0 and r.m.s.d. 3.4 Å). This relatively large r.m.s.d. spread between *Ph*Pth2 and *Af*Pth2 may reflect the relative accuracy of crystal and solution structures (Smith *et al.*, 1994). If only C$^\alpha$ atoms in the four β-strands that make up the hydrophobic core are included in the comparison, the r.m.s.d. value is about 1.7 Å. Similar features in the comparison of crystal and solution structures have also been reported for other proteins (Billeter *et al.*, 1989; Clore & Gronenborn, 1991; Berndt *et al.*, 1992). According to the reported site-directed mutagenesis experiment on *Ss*Pth2 (Fromant *et al.*, 2005), three conserved residues, Lys23 in the α1 helix and Asp87 and Thr91 in the β3–β4 loop, are expected to form the active site (Fig. 3). The residues which make up the dimer interface are well conserved, indicating the importance of these residues for dimeric association; seven of 23 (total) or five of 13 (core) interface residues in *Ph*Pth2 are invariant. Notably, all Pth2-family members of known structure (*Ph*Pth2, hPth2, *Ss*Pth2 and *Ta*Pth2) make similar biological dimers with a common inter-protomer assembly (Fig. 4). Each asymmetric unit of the hPth2 and *Ss*Pth2 crystal structures contains two and four protomers, respectively, and these protomers form the common dimers with noncrystallographic twofold axes. On the other hand, the asymmetric unit of the *Ta*Pth2 crystal structure contains a protomer and the crystallographic twofold axis produces the common dimer. This conservation of overall dimeric assembly suggests biological importance of the dimeric state in Pth2-family enzymes.

3.3. Thermostability

The correlation between the structure and the thermodynamic stability was investigated by evaluating the Gibbs free energy, number of ion pairs and entropy of the determined crystal structures of *Ph*Pth2 and comparing them with those of Pth2-family members. The change in Gibbs free energy (ΔG) between different states (denatured *versus* monomeric states and monomeric *versus* dimeric states) was calculated using the following three procedures. (i) ΔG was calculated from the accessible surface area (ASA) of nonpolar (C and S) and polar (N and O) atoms (Funahashi *et al.*, 1999). The differences in the ASA value between two states,

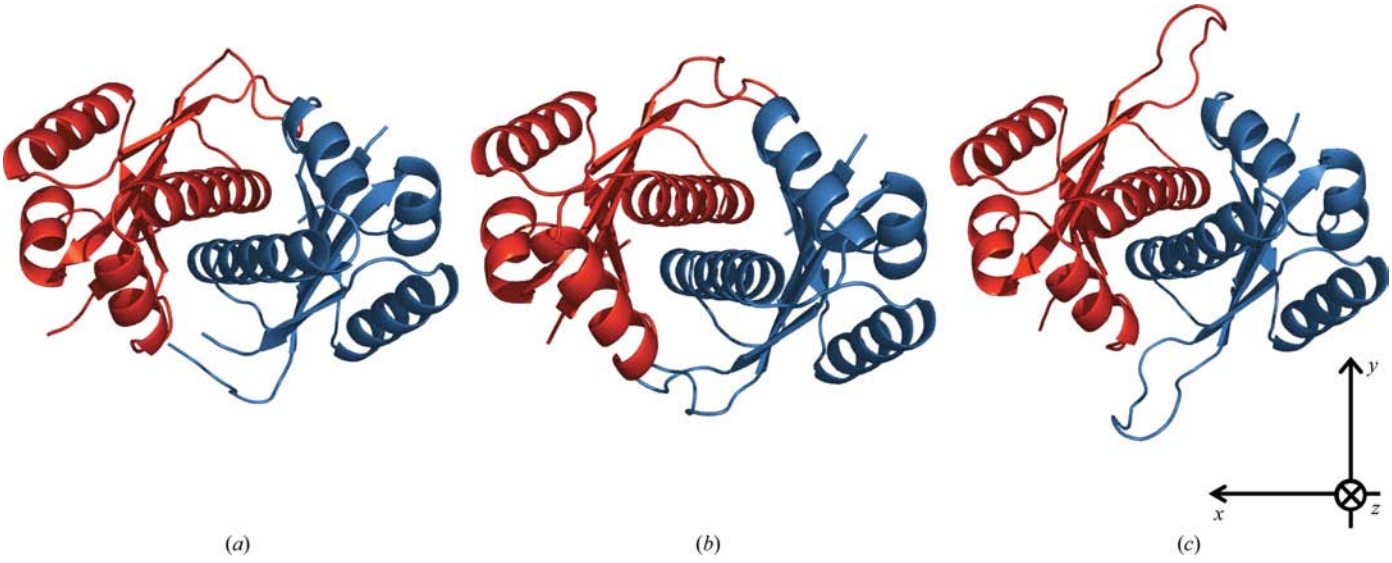

Figure 4
Ribbon diagrams of Pth2 dimers: (*a*) hPth2, (*b*) *Ss*Pth2 and (*c*) *Ta*Pth2. For comparison with other figures, the direction of the projection is shown by the coordinate axes. This figure was generated using *PyMOL* (DeLano, 2002).

Table 2
The contribution of intra-protomer interaction to the thermal stability of Pth2 family members.

ΔG_i and $\Delta\Delta G_i$ (i = np, p or e) values upon denaturation are shown in kJ mol^{-1}. $\Delta\Delta G_i$ represents the difference in ΔG_i between *Ph*Pth2 form 1 and the other Pth2-family members. T_{ogt} is the optimal growth temperature.

				Nonpolar interaction				Polar interaction							
				ΔASA (Å^2)				Ion pairs (<5 Å)	Hydrogen bond			Entropy		Total ΔΔG	
	T_{ogt} (K)	No. of residues	Protomer ASA (Å^2)	C/S	N/O	ΔG_{np}	$\Delta\Delta G_{np}$	No.	No.	ΔG_p	$\Delta\Delta G_p$	ΔG_e ($-T\Delta S$)†	$\Delta\Delta G_e$	$\Delta\Delta G_{np}$ + $\Delta\Delta G_p$ + $\Delta\Delta G_e$	
*Ph*Pth2 (form 1)	368	121	6897	7085	2789	1225	0	17	251	2134	0	−79	0	0	
*Ph*Pth2 (form 2)‡	368	121	6758	7079	2875	1223	−2	18	264	2244	110	−79	0	108	
*Ss*Pth2§	358	120	6661	7373	2923	1274	49	8	264	2244	110	−18	61	220	
*Ta*Pth2¶	333	117	6825	6927	2945	1195	−30	23	256	2176	42	−33	46	58	
hPth2††	310	117	6429	7053	2886	1217	−8	8	247	2100	−34	−27	52	10	

† Values of ΔG_e were calculated at 310 K. ‡ The averaged ΔASA value for two subunits was used. § The model used was 1xty from the PDB. The averaged ΔASA value for four subunits was used. ¶ The model used was 1rlk from the PDB. †† The model used was 1q7s from the PDB. The averaged ΔASA value for two subunits was used.

Table 3
The contribution of inter-protomer interaction to the thermal stability of Pth2-family members.

ΔG_i and $\Delta\Delta G_i$ (i = np or p) values are shown in kJ mol^{-1}. $\Delta\Delta G_i$ represents the difference in ΔG_i between *Ph*Pth2 form 1 and the other Pth2-family members. The intersubunit nonpolar interactions were calculated using the following formula: $\Delta G_{np} = \alpha\Delta ASA_{nonpolar} + \beta\Delta ASA_{polar}$, where $\Delta ASA_{nonpolar}$ = ASA(C/S, subunit *A*) + ASA(C/S, subunit *B*) − ASA(C/S, dimer *AB*), ΔASA_{polar} = ASA(N/O, subunit *A*) + ASA(N/O, subunit *B*) − ASA(N/O, dimer *AB*), α = 0.178 and β = −0.013. The same procedure was employed for dimer *CD* in *Ss*Pth2. The models used in the calculation are the same as those in Table 2.

			Nonpolar interaction				Polar interaction				
			ΔASA (Å^2)				Hydrogen bond			Ion pair (<5 Å)	Total ΔΔG
	Dimer ASA (Å^2)	Dimer interface (Å^2)	C/S	N/O	ΔG_{np}	$\Delta\Delta G_{np}$	No.	ΔG_p	$\Delta\Delta G_p$	No.	$\Delta\Delta G_{np}$ + $\Delta\Delta G_p$
*Ph*Pth2 (form 1)	11730	1026	1550	487	270	0	6	51	0	0	0
*Ph*Pth2 (form 2)	11194	1101	1721	485	300	30	6	51	0	0	30
*Ss*Pth2 (dimer *AB*)	11452	953	1488	379	260	−10	4	34	−17	0	−27
*Ss*Pth2 (dimer *CD*)	11413	937	1464	374	256	−14	2	17	−34	0	−48
*Ta*Pth2	11406	1112	1583	618	274	4	10	85	34	0	38
hPth2	10643	1085	1358	770	232	−38	6	51	0	2	−38

$\Delta ASA_{nonpolar}$ and ΔASA_{polar}, were used in calculations using the following relationship: $\Delta G = \alpha\Delta ASA_{nonpolar} + \beta\Delta ASA_{polar}$, where $\alpha = 0.178$ and $\beta = -0.013$. The ASA values in the monomeric and dimeric native states were calculated using a previously reported procedure (Connolly, 1993). Extended structures were generated using the *INSIGHT II* software (Accelrys Inc.) and used for the calculation of ASA values in the denatured state. (ii) ΔG was calculated from the net contribution of hydrogen bonds. Takano *et al.* (1999) reported the net contribution of an intramolecular hydrogen bond to the conformational stability to be 8.5 kJ mol^{-1} for a hydrogen bond of length 3 Å. Thus, ΔG can be calculated as $\Delta G = 8.5N_{HB}$, where N_{HB} is the number of hydrogen bonds. (iii) ΔG was calculated from the entropic effect. Oobatake & Ooi (1993) proposed that the entropic effect upon denaturation (ΔS) arising from the side chains of the amino-acid residues can be calculated from the thermodynamic parameters for 20 amino-acid residues. ΔG can simply be calculated as follows: $\Delta G = -T\Delta S$, where T is the absolute temperature.

The hydrophobic interaction in the interior of a protein (Kauzmann, 1959) and the ion-pair network on the protein surface are thought to be important stabilizing factors (Hennig *et al.*, 1995; Yip *et al.*, 1995; Pappenberger *et al.*, 1997). The thermodynamic parameters of intra-protomer interaction arising from the nonpolar interaction, polar interaction and entropic effect for Pth2-family members are listed in Table 2. In the total $\Delta\Delta G$ values, *Ss*Pth2 (T_{ogt} = 358 K) shows the highest value of 220 kJ mol^{-1}. However, the number of ion pairs in *Ph*Pth2 (T_{ogt} = 368 K) is 17 in form 1 and 18 in form 2, which is approximately ten more than the number of ion pairs in *Ss*Pth2. The higher number of ion pairs may compensate for the total $\Delta\Delta G$ value and contribute to the higher thermostability of *Ph*Pth2. The value of $\Delta\Delta G$ and the number of ion pairs of *Ta*Pth2 are comparable to those in *Ph*Pth2. Considering the function of *T. acidophilum* in an acidic environment (pH 0.5–4), additional stability of *Ta*Pth2 (T_{ogt} = 333 K) may be required. Both the $\Delta\Delta G$ value and the number of ion pairs are low in hPth2 (T_{ogt} = 310 K), suggesting the lowest stability of all the family members. In order to evaluate the correlation between the dimeric structure and thermostability, thermodynamic parameters, the dimer ASA and the dimensions of the buried dimer interface were calculated for the Pth2-family members (Table 3). The values of the dimer ASA, dimer-interface dimensions and the numbers of hydrogen bonds and ion pairs do not show any correlation with the optimum growth temperatures of the source organisms. Considering the difference in the total $\Delta\Delta G$ value of 30 kJ mol^{-1} between *Ph*Pth2 form 1 and form 2, there is no significant difference between the hyperthermophilic archeon *Ph*Pth2 and other

Table 4
Multiple C$^{\alpha}$ superposition of *Ph*Pth2 dimer.

The annotation of each molecule is the same as that in the caption of Fig. 5.

		Secondary fitting†							
		Rigid-body shift							Local shift
Primary fitting‡			Rotation axis (°)		Rotation (°)				
Fitted part	R.m.s.d. (Å)	Fitted part	ω	φ	χ	Axis–centroid distance (Å)	Residue of least shift	R.m.s.d. (Å)	R.m.s.d. (Å)
F2(*A*, *B*)→F1(*A*, sym*A*)	0.52	F2_*A*→F1_*A*	116.5	76.5	1.3	4.3	Ile11	0.25	0.39
		F2_*B*→F1_sym*A*	119.5	−89.1	1.8	3.0	Ile11	0.31	0.48

† After the primary fitting, the indicated form 2 dimer was fitted again and the applied rotations were listed in spherical polar angles. Axis–centroid distance is the distance between the rotational axis and the centroid of the protomer used in the secondary fitting. The rotational axis passes in the vicinity of the indicated residues with the least rigid-body shift. The definition of spherical polar angles is as described in Collaborative Computational Project, Number 4 (1994). ‡ C$^{\alpha}$ atoms of the form 2 dimer were superimposed on those of the form 1 dimer.

organisms. These features suggest that the dimeric structure does not make a major contribution to the thermostabilization of this enzyme, but that the total number of ion pairs plays a crucial role. These results are reminiscent of oligomeric enzymes such as glycine-cleavage system T-protein (Lokanath *et al.*, 2005) and dehydroquinate synthase (Sugahara *et al.*, 2005), in which the interface residues are well conserved and the interface area does not change according to the growth temperature of the source organism, thereby suggesting the catalytic relevance of the oligomerization. By analogy, the Pth2 dimerization might be required for catalysis by affecting the active-site conformation, rather than for its contribution to thermostability.

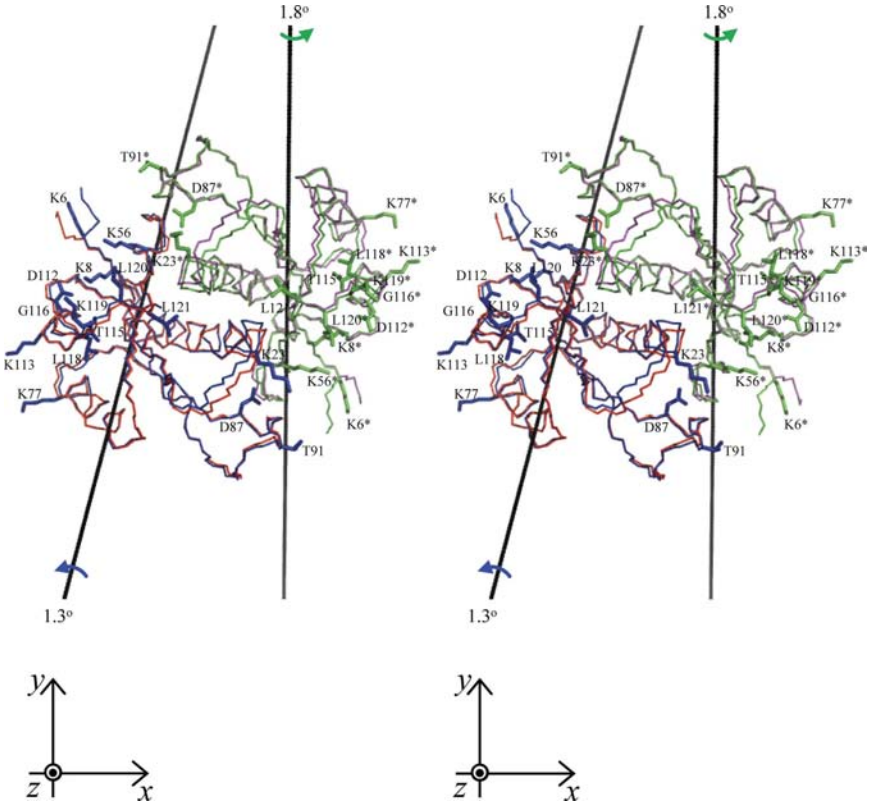

Figure 5
Stereoview of the C$^{\alpha}$ superposition after primary fitting. The whole of the form 2 dimer is superimposed onto the whole of the form 1 dimer. Each molecule is coloured red (subunit *A* of form 1; F1_*A*), magenta (crystal symmetry-related subunit *A* of form 1; F1_sym*A*), blue (subunit *A* of form 2; F2_*A*) and green (subunit *B* of form 2; F2_*B*). The putative tRNA-recognition residues are depicted as stick models with subunit colourings. The residues of F1_sym*A* are marked with asterisks. The rigid-body rotation of each subunit in the form 2 dimer from the corresponding subunit in the form 1 dimer with perfect twofold symmetry is represented by a black axis with a blue (F1_*A* to F2_*A*) or a green (F1_sym*A* to F2_*B*) arrow indicating the direction of rotation. For comparison with other figures, the direction of the projection is shown by the coordinate axes. This figure was generated using *PyMOL* (DeLano, 2002).

3.4. Implication of the conformational change upon ligand binding

In general, the substrate recognition of enzymes involves a conformational change upon ligand binding. In recent work, we observed a subtle structural difference by multiple C$^{\alpha}$ superposition between several liganded and unliganded forms and clarified the structural change of the phenylacetate-degradation protein PaaI upon ligand binding (Kunishima *et al.*, 2005). In order to understand the mechanism of substrate recognition in *Ph*Pth2, we tried to follow the same technique to quantitatively evaluate the observed structural difference between the form 1 and 2 dimers. The form 1 dimer, the protomers of which are related by the crystallographic twofold axis, was used as a reference for the superposition and the form 2 dimer was superimposed onto the form 1 dimer in two steps: primary fitting and secondary fitting. In the primary fitting, all C$^{\alpha}$ atoms of the form 2 dimer were superimposed on the form 1 dimer so as to minimize the r.m.s.d. between the two dimers. After the primary fitting, the superimposed *A* and *B* subunits of the form 2 dimer were individually fitted again onto the

A subunit and crystal-symmetry-related *A* subunit (sym*A*) of the form 1 dimer, respectively (secondary fitting). The structural difference between two forms can be described by a combination of an inter-protomer rigid-body rearrangement of the subunit referred to as a rigid-body shift and an intra-protomer local deformation of the polypeptide chain referred to as a local shift. The rigid-body shift of a subunit with respect to the reference subunit can be precisely described by a rotation about an axis passing across the subunit.

A summary of the multiple C^{α} superposition analysis is shown in Table 4. In the primary fitting, the r.m.s.d. value of 0.52 Å between the form 1 and form 2 dimers is substantially larger than the value of the estimated coordinate errors from the Luzzati plot (Table 1), suggesting significant conformational differences between the two dimers. In the secondary fitting, the rotation axis for the rigid-body shift passes through a point in the vicinity of Ile11, which is close to the centroid of each protomer. The rotation axis–centroid distances are 4.3 Å for the superposition F2_*A* to F1_*A* and 3.0 Å for the superposition F2_*B* to F1_sym*A* (Fig. 5). The r.m.s.d.s for the rigid-body and local shifts are comparable, indicating that both the shifts of protomers contribute to the whole conformational change of the dimer. The rotation angles χ of the rigid-body shift are 1.3° for the superposition F2_*A* to F1_*A* and 1.8° for the superposition F2_*B* to F1_sym*A*, which are comparable to those in the reported study of PaaI (Kunishima *et al.*, 2005), in which 1.2–2.0° rigid-body rotations in the secondary fitting between various liganded forms and the reference unliganded form were observed. Importantly, the present C^{α} superposition analysis indicates that the rotation axis ($\omega\varphi$) of the rigid-body rotation is approximately perpendicular to the twofold symmetry of the dimer. Thus, the rigid-body rotation tends to maintain the twofold axis of the dimer, suggesting positive cooperativity upon ligand binding. Assuming that this observed tendency of the rigid-body rotation is also true in the conformational change upon ligand binding, the ligand tRNA may bind to both the putative active sites of the *Ph*Pth2 dimer with positive cooperativity. In contrast, Kishishita *et al.* (2008) present an opposite strategy for ligand recognition in the archaeal diphthine synthase (DS) dimer, in which the rotation axis ($\omega\varphi$) of the rigid-body rotation upon ligand binding is not perpendicular to the crystallographic twofold axis of the dimer. This arrangement between the rotation axis and the dimeric twofold axis tends to break the dimeric twofold symmetry by the χ-axis rotation, indicating that negative cooperativity will occur for the ligand binding. As a result, only

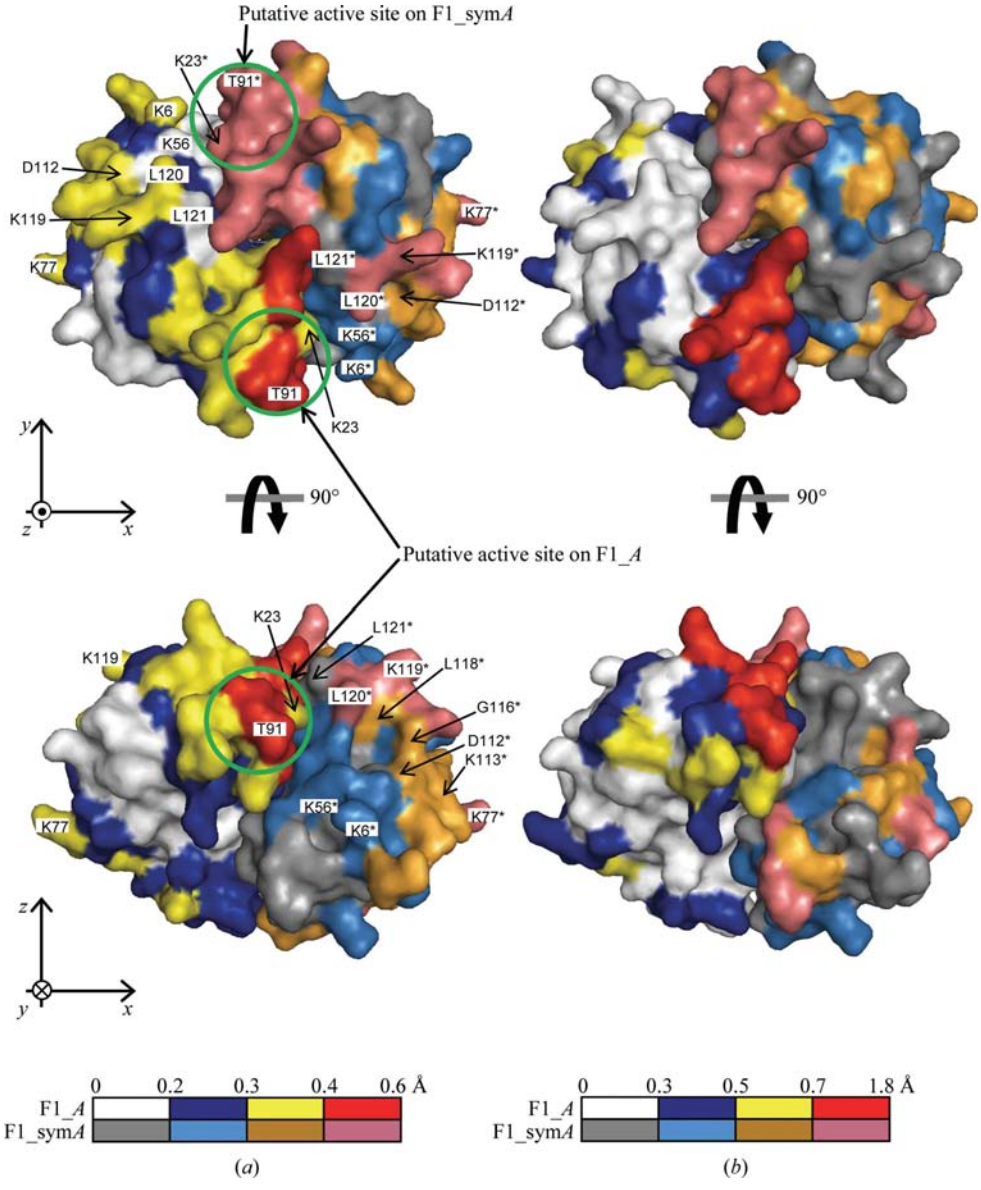

Figure 6
Localization of positional shifts in the secondary fitting. The annotation of each molecule is as defined in the caption of Fig. 5. The positional shifts of C^{α} atoms are categorized into (*a*) rigid-body shifts and (*b*) local shifts. The shifts from the superpositions F2_*A* to F1_*A* and F2_*B* to F1_sym*A* are mapped by residue on the molecular surfaces of F1_*A* and F1_sym*A*, respectively. The magnitude of the shifts is colour-coded as indicated. Orthogonal views are shown in the upper and lower panels. The putative tRNA-recognition residues and the putative active sites are labelled in (*a*). For comparison with other figures, the directions of the projections for the upper and lower panels are shown by the coordinate axes. The molecular surface was generated using *PyMOL* (DeLano, 2002).

one of the two active sites in the DS dimer is occupied by ligand. Both DS and *Ph*Pth2 work as a dimer and need to recognize large substrates: elongation factor 2 and tRNA, respectively. For this purpose, these enzymes adopt completely opposite strategies for ligand binding. In DS, when elongation factor 2 binds at one of the two active sites, the affinity of the other active site decreases owing to the negative cooperativity. Hence, only one ligand is precisely recognized by the dimer by sacrificing one of the two active sites. In *Ph*Pth2, on the other hand, when the peptidyl-tRNA binds at one of the two active sites the affinity of the other active site becomes higher owing to positive cooperativity, allowing ligand binding at both active sites.

In order to visualize the conformational change, the positional shifts of all C^{α} atoms for the superposition of F2_*A* onto F1_*A* as well as of F2_*B* onto F1_sym*A* were mapped onto the molecular surface of the form 1 *Ph*Pth2 dimer (Fig. 6). The residues with larger positional shifts mainly aggregate around the putative active site and this region includes residues Lys23, Asp87 and Thr91. These residues are expected to form the active site and are conserved in all Pth2-family members examined in the present study (enclosed in a box in Fig. 3), suggesting the practical importance of these residues upon ligand binding. Therefore, the present analysis shows that the putative active sites of *Ph*Pth2 are flexible and that the flexibility is derived from both rigid-body and local shifts of subunits.

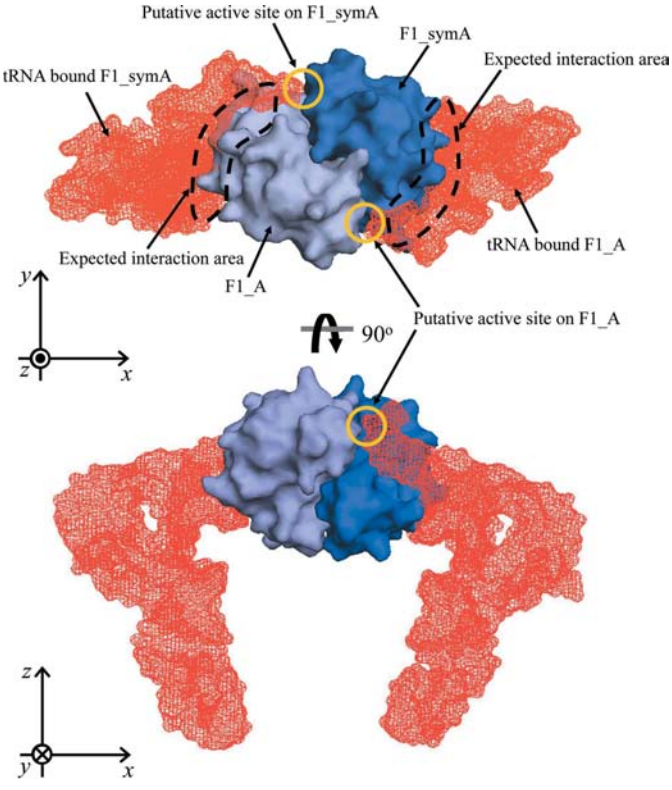

Figure 7
Docking model of *Ph*Pth2 form 1 dimer and *Saccharomyces* tRNA. The *Ph*Pth2 dimer is coloured light blue (subunit *A*; F1_*A*) and dark blue (crystal symmetry-related subunit *A*; F1_sym*A*) and tRNA molecule is presented as a red mesh. Orthogonal views are shown in the top and bottom panels. For comparison with other figures, the direction of the projection is shown by the coordinate axes. The molecular surface was generated using *PyMOL* (DeLano, 2002).

In order to explore the substrate recognition of *Ph*Pth2, we made a manual docking model of the *Ph*Pth2 dimer with phenylalanine tRNA (PDB code 1evv; Fig. 7). In the catalytic reaction, the 3′ terminus of the tRNA must be located in the vicinity of the active site within a distance short enough for peptidyl-tRNA hydrolysis. To make a manual docking model, we fixed the 3′ terminus of tRNA in the putative active site, composed of the invariant active-site residues Lys23, Asp87 and Thr91, so as to provide the best fit without steric clashes. On the surface of the docking region, the basic residues Lys6, Lys8, Lys23, Lys56, Lys77 and Lys113 were observed, suggesting the biological reality of this model. Of these residues, Lys8, Lys23 and Lys113 are well conserved in the Pth2-family members. Furthermore, the ten C-terminal residues of *Ph*Pth2 (residues 112–121) make an additional interaction area with the tRNA molecule in which residues Asp112, Thr115, Gly116 and Leu120 are invariant and residues Lys113, Leu118, Lys119 and Leu121 are well conserved in the Pth2-family members. Importantly, from the docking model, one molecule of the large substrate peptidyl-tRNA has to be recognized by both subunits of the *Ph*Pth2 dimer (Figs. 5, 6 and 7): the invariant active-site residues Lys23, Asp87 and Thr91 from one protomer and other basic or C-terminal recognition residues from the other protomer. This notion indicates the biological importance of the dimeric state in the Pth2-family enzymes.

4. Conclusion

Crystal structures of peptidyl-tRNA hydrolase 2 from *P. horikoshii* OT3 (*Ph*Pth2) have been determined in two different crystal forms. Both forms contain a biological dimer and the protomer has high sequence identity to and shares the same topology with previously reported structures of Pth2-family members. A semi-empirical evaluation of the protein thermodynamic stability of *Ph*Pth2 was made and was compared with those of other Pth2-family members. The abundant number of ion pairs compared with family members from other mesophilic organisms may contribute to the thermostability of *Ph*Pth2. The multiple superposition analysis elucidated the structural flexibility of the *Ph*Pth2 dimer quantitatively and revealed that the structural difference was remarkable around the putative active site. This analysis also suggested positive cooperativity upon ligand binding. The mechanism of substrate recognition was further investigated using a docking model with a tRNA molecule, in which both subunits of the *Ph*Pth2 dimer cooperate to recognize one L-shaped tRNA molecule. It is probable that the *Ph*Pth2 dimer binds two tRNA molecules simultaneously according to the twofold dimeric symmetry, indicating positive inter-protomer cooperativity on substrate binding which might be linked to an *in vivo* requirement. Considering that the function of Pth2 is the renaturation of tRNA from the useless substrate peptidyl-tRNA, a possible biological role of the

positive cooperativity is feed-forward activation of Pth2 according to the concentration of peptidyl-tRNA, which can be varied depending upon the emergency level in the cell. Further experimental investigation is needed for a conclusive understanding of the substrate-recognition mechanism of this enzyme.

Of the authors, KS made the main contribution to the work and wrote the paper, CK contributed to the large-scale protein production, MS contributed to the automatic crystallization screening and NK supervised the work. The authors thank the staff of RIKEN Genomic Science Center for providing the plasmid, the technical staff of RIKEN SPring-8 Center for assistance in the large-scale protein production and the dynamic light-scattering experiment and the beamline staff at BL26B1 and BL26B2 of SPring-8 for assistance during data collection. The present study (PH1539/HTPF10720) was supported by the 'National Project on Protein Structural and Functional Analyses' funded by the MEXT of Japan.

References

Altschul, S. F., Gish, W., Miller, W., Myers, E. W. & Lipman, D. J. (1990). *J. Mol. Biol.* **215**, 403–410.
Berndt, K. D., Güntert, P., Orbons, L. P. M. & Wüthrich, K. (1992). *J. Mol. Biol.* **227**, 757–775.
Billeter, M., Kline, A. D., Braun, W., Huber, R. & Wüthrich, K. (1989). *J. Mol. Biol.* **206**, 677–687.
Brun, G., Paulin, D., Yot, P. & Chapeville, F. (1971). *Biochimie*, **53**, 225–231.
Brünger, A. T., Adams, P. D., Clore, G. M., DeLano, W. L., Gros, P., Grosse-Kunstleve, R. W., Jiang, J.-S., Kuszewski, J., Nilges, M., Pannu, N. S., Read, R. J., Rice, L. M., Simonson, T. & Warren, G. L. (1998). *Acta Cryst.* D**54**, 905–921.
Chayen, N. E., Shaw Stewart, P. D., Maeder, D. L. & Blow, D. M. (1990). *J. Appl. Cryst.* **23**, 297–302.
Clore, G. M. & Gronenborn, A. M. (1991). *J. Mol. Biol.* **221**, 47–53.
Collaborative Computational Project, Number 4 (1994). *Acta Cryst.* D**50**, 760–763.
Connolly, M. L. (1993). *J. Mol. Graph.* **11**, 139–141.
DeLano, W. L. (2002). *The PyMOL Molecular Graphics System.* http://www.pymol.org.
Fromant, M., Ferri-Fioni, M. L., Plateau, P. & Blanquet, S. (2003). *Nucleic Acids Res.* **31**, 3227–3235.
Fromant, M., Schmitt, E., Mechulam, Y., Lazennec, C., Plateau, P. & Blanquet, S. (2005). *Biochemistry*, **44**, 4294–4301.
Funahashi, J., Takano, K., Yamagata, Y. & Yutani, K. (1999). *Protein Eng.* **12**, 841–850.
Hennig, M., Darimont, B., Sterner, R., Kirschner, K. & Jansonius, J. N. (1995). *Structure*, **3**, 1295–1306.
Holm, L. & Sander, C. (1997). *Nucleic Acids Res.* **25**, 231–234.
Kauzmann, W. (1959). *Adv. Protein Chem.* **14**, 1–63.
Kössel, H. (1970). *Biochim. Biophys. Acta*, **204**, 191–202.
Kishishita, S., Shimizu, K., Murayama, K., Terada, T., Shirouzu, M., Yokoyama, S. & Kunishima, N. (2008). *Acta Cryst.* D**64**, 397–406.
Kunishima, N., Asada, Y., Sugahara, M., Ishijima, J., Nodake, Y., Sugahara, M., Miyano, M., Kuramitsu, S., Yokoyama, S. & Sugahara, M. (2005). *J. Mol. Biol.* **352**, 212–228.
Kwong, P. D. & Liu, Y. (1999). *J. Appl. Cryst.* **32**, 102–105.
Laskowski, R. A., MacArthur, M. W. & Thornton, J. M. (1998). *Curr. Opin. Struct. Biol.* **8**, 631–639.
Lokanath, N. K., Kuroishi, C., Okazaki, N. & Kunishima, N. (2005). *Proteins*, **58**, 769–773.
Meinnel, T., Mechulam, Y. & Blanquet, S. (1993). *Biochimie*, **75**, 1061–1075.
Menez, J., Buckingham, R. H., de Zamaroczy, M. & Campelli, C. K. (2002). *Mol. Microbiol.* **45**, 123–129.
Menninger, J. R. (1976). *J. Biol. Chem.* **251**, 3392–3398.
Oobatake, M. & Ooi, T. (1993). *Prog. Biophys. Mol. Biol.* **59**, 237–284.
Otwinowski, Z. & Minor, W. (1997). *Methods Enzymol.* **276**, 307–326.
Pappenberger, G., Schurig, H. & Jaenicke, R. (1997). *J. Mol. Biol.* **274**, 676–683.
Pereda, J. M. de, Waas, W. F., Jan, Y., Ruoslahti, E., Schimmel, P. & Pascual, J. (2004). *J. Biol. Chem.* **279**, 8111–8115.
Powers, R., Mirkovic, N., Goldsmith-Fischman, S., Acton, T. B., Chiang, Y., Huang, Y. J., Ma, L., Rajan, P. K., Cort, J. R., Kennedy, M. A., Liu, J., Rost, B., Honig, B., Murray, D. & Montelione, G. T. (2005). *Protein Sci.* **14**, 2849–2861.
Rosas-Sandoval, G., Ambrogelly, A., Rinehart, J., Wei, D., Cruz-Vera, L. R., Graham, D. E., Stetter, K. O., Guarneros, G. & Söll, D. (2002). *Proc. Natl Acad. Sci. USA*, **99**, 16707–16712.
Schmitt, E., Mechulam, Y., Fromant, M., Plateau, P. & Blanquet, S. (1997). *EMBO J.* **16**, 4760–4769.
Sugahara, M. & Miyano, M. (2002). *Tanpakushitsu Kakusan Koso*, **47**, 1026–1032.
Sugahara, M., Nodake, Y., Sugahara, M. & Kunishima, N. (2005). *Proteins*, **58**, 249–252.
Smith, L. J., Redfield, C., Smith, R. A. G., Dobson, C. M., Clore, G. M., Gronenborn, A. M., Walter, M. R., Naganbushan, T. L. & Wlodawer, A. (1994). *Nature Struct. Biol.* **1**, 301–310.
Takano, K., Yamagata, Y., Funahashi, J., Hioki, Y., Kuramitsu, S. & Yutani, K. (1999). *Biochemistry*, **38**, 12698–12708.
Ueno, G., Hirose, R., Ida, K., Kumasaka, T. & Yamamoto, M. (2004). *J. Appl. Cryst.* **37**, 867–873.
Ueno, G., Kanda, H., Hirose, R., Ida, K., Kumasaka, T. & Yamamoto, M. (2006). *J. Struct. Funct. Genomics*, **7**, 15–22.
Vagin, A. & Teplyakov, A. (1997). *J. Appl. Cryst.* **30**, 1022–1025.
Yip, K. S. P., Stillman, T. J., Britton, K. L., Artymiuk, P. J., Baker, P. J., Sedelnikova, S. E., Engel, P. C., Pasquo, A., Chiaraluce, R., Consalvi, V., Scandurra, R. & Rice, D. W. (1995). *Structure*, **3**, 1147–1158.